

# VEnvision3D: A Synthetic Perception Dataset for 3D Multi-Task Model Research

Jiahao Zhou<sup>1†</sup>, Chen Long<sup>2†</sup>, Yue Xie<sup>2</sup>, Jialiang Wang<sup>1</sup>,  
Boheng Li<sup>3</sup>, Haiping Wang<sup>2</sup>, Zhe Chen<sup>2\*</sup>, Zhen Dong<sup>2</sup>

<sup>1</sup> School of Remote Sensing and Information Engineering, Wuhan University, China

<sup>2</sup> State Key Laboratory of Information Engineering in Surveying,  
Mapping and Remote Sensing, Wuhan University, China

<sup>3</sup> Key Laboratory of Aerospace Information Security and Trusted Computing,  
Ministry of Education, School of Cyber Science and Engineering, Wuhan University, China

<sup>†</sup> Equal contribution \* Corresponding author.

## Abstract

*Developing a unified multi-task foundation model has become a critical challenge in computer vision research. In the current field of 3D computer vision, most datasets solely focus on a relatively limited set of tasks, which complicates the concurrent training requirements of various downstream tasks. This makes the training of multi-objective networks difficult to proceed with, which further hinders the development of foundation models in the 3D vision field. In this paper, we introduce VEnvision3D, a large 3D synthetic perception dataset for multi-task learning, including depth completion, segmentation, upsampling, place recognition, and 3D reconstruction. Since the data for each task was collected in the same scenarios, tasks are inherently aligned in terms of the utilized data. Therefore, such a unique attribute can assist in exploring the potential for the multi-task model and even the foundation model without separate training methods. Several new benchmarks based on the characteristics of the proposed dataset were presented. Extensive studies were performed on end-to-end models, revealing new observations, challenges, and opportunities for future research. In addition, we designed a straightforward multi-task network to uncover the ability that VEnvision3D can offer for the foundation model. Our dataset and code will be open-sourced upon acceptance.*

## 1. Introduction

The development of AI models has made many novel tasks possible. Previously, it was inconceivable that AI could autonomously imitate human creativity; however, Voice-Box [33] and DALLE-2 [50] are now capable of independently generating audio and images. Recently, foundation models (trained on a vast quantity of data at scale such

that they can be adapted to a wide range of downstream tasks)[6] have once again sparked transformative revolutions across diverse industries. Examples include CLIP [49] and SAM [31] in computer vision, GPT-4 [42] in natural language processing, as well as UniAD [27] in autonomous driving. *Multi-task, unified, end-to-end* frameworks have become the new direction for the foundation model.

The development of these models has benefited from the improvement of computing power, algorithm optimization, and the emergence of large-scale, high-quality data [73], such as the widely successful ImageNet [12] and Instruct-GPT [43]. Thanks to the availability of large-scale 2D image datasets and relatively small domain shifts between images [72], the development of the foundation model in 2D computer vision has become relatively mature. However, due to a relatively late start, we lack a large number of available datasets in 3D computer vision. As shown in Fig. 1, with a significantly smaller quantity of datasets compared to datasets in the 2D domain, some mainstream datasets also have much smaller scales [4, 9, 12, 17, 37, 38].

In the case of insufficient datasets, different parameter designs of 3D sensors result in a domain gap in 3D data that is much larger than that in 2D images, which further complicates the integration of the 3D data. Currently, a singular dataset is typically limited to specific downstream tasks. For example, the SemanticKITTI [4] dataset provides large-scale annotated point clouds, but the fixed collection route makes it unable to be used for place recognition tasks. Such a situation forces us to train multiple networks separately on different datasets, which not only affects the efficiency and accuracy of multi-task models but also limits the exploration of inter-task relationships [61]. Multi-task learning is considered the earliest attempt of the foundation model [16, 55]. However, the current situation of insufficient quantity of 3D datasets and the difficulty of data in-

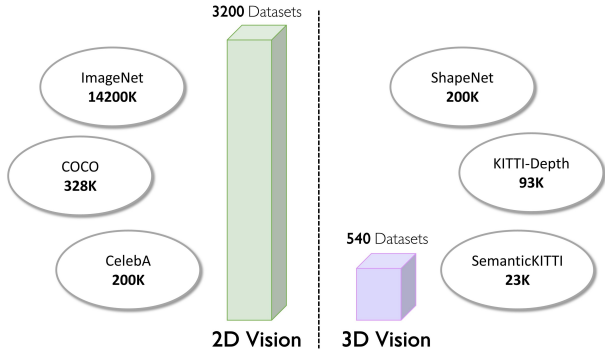


Figure 1. A comparison between dataset quantities in 2D and 3D vision and the data volume of classic datasets across different domains. The statistic data is from the Papers With Code[1] website.

tegration makes the research on 3D multi-task learning extremely challenging. Subsequently, this further impedes the development of foundation models in the 3D vision domain.

A dataset collected within the same scenarios is required for investigating the relationships among subtasks, which can offer fresh insights in the development of 3D vision foundation models. In this paper, we introduce the VEnvision3D dataset, facilitating the exploration of multi-task models and the relationships between tasks in the field of 3D Vision, including depth completion, segmentation, up-sampling, place recognition, and 3D reconstruction. Collected in CARLA Simulator [15], we divide the dataset into several subset by specific task. Meanwhile, based on the characteristics of virtual environments, the dataset provides functionalities that real datasets cannot provide, such as simulating temporal changes in the environment and sampling point clouds on model surfaces. This expands the range of scenarios and variation factors for evaluating algorithm performance, enabling more comprehensive exploration of their robustness and adaptability.

Additionally, We conducted experiments to investigate the mutually beneficial relationships among specific subtasks. The experimental results revealed that this mutually beneficial relationship can improve the accuracy of subtasks. Beyond the scope of multi-task model development, we believe that a versatile dataset can assist researchers in exploring the potential for unified foundation models. Thus, we can offer a platform that fosters innovation for researchers(See Fig. 2), unifies the target tasks within the field of 3D Vision, and ultimately achieve a *Foundation Model of Future-oriented Artificial General Intelligence*.

The main contributions of our work are summarized as follows:

- We introduce the VEnvision3D dataset, the first synthetic dataset that allows validation of multiple tasks within the same scenario.

	Dataset	Cities	Task				
			Dep.	Ups.	Seg.	Recg.	Recs.
Real-world	KITTI [17]	1	✓				✓
	SemanticKITTI [4]	1			✓		
	ShapeNet [9]	object		✓	✓		✓
	Oxford RobotCar [40]	1				✓	✓
	S3DIS [3]	indoor			✓		
Synthetic	SynthCity [18]	1			✓		
	STPLS3D [10]	aerial			✓		
	KITTI-CARLA [13]	8	✓		✓		✓
	AIODrive [64]	8	✓		✓		
	SHIFT [56]	8	✓				✓
<b>Ours</b>		8	✓	✓	✓	✓	✓

Table 1. Comparison of supported tasks of existing 3D point cloud datasets. VEnvision3D is the only dataset that simultaneously supports depth completion(Dep.), segmentation(Seg.), upsample(Ups.), place recognition(Recg.), and 3D reconstruction(Recs.) in the same environmental domain.

- The data collected in virtual environments yields novel attributes that are difficult to acquire in real-world situations, thereby offering fresh insights.
- Using our dataset, we designed a straightforward multi-task network designed to demonstrate the mutual benefits among different tasks, highlighting the dataset’s versatility and potential to advance foundation model research.

## 2. Related Works

Numerous datasets have been proposed in the past. However, they often exhibit limitations by being restricted to a single functionality. Tab. 1 shows the functionalities provided by current mainstream datasets. The following chapter presents a compilation of several renowned datasets.

**Depth Completion.** KITTI DC [58] is a widely used large-scale outdoor dataset that contains over 93,000 semi-dense depth maps with the corresponding raw sparse LiDAR scans and RGB images [23]. The DenseLivox [70] dataset is collected with much denser depth maps than KITTI. DeepLiDAR [48] provides a synthetic dataset generated by the CARLA Simulator [15]. Our dataset provides accurate ground truth depth obtained through rendering and point cloud projections with varying densities in the same frame.

**Upsample.** There are various point cloud datasets [5, 9, 60, 65] used to evaluate the performance of point cloud up-sampling algorithms. Researchers usually downsample the ground truth as the input. Some researchers choose to build their dataset for training and testing of point cloud up-sampling models [34, 46, 47, 68, 69]. Compared to ours, these datasets do not provide data collected in large-scale outdoor scenes.

**Segmentation.** For real-world datasets, SemanticKITTI [4] provides point-wise annotated point clouds. Recently,



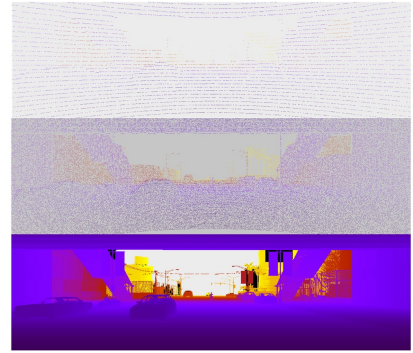
### 3D Reconstruction

Provide city-level mesh models as a new benchmark



### Place Recognition

Provide data before and after environment migration



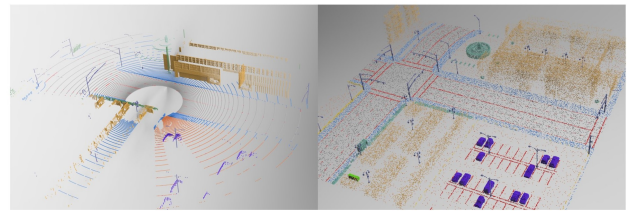
### Depth Completion

Provide point cloud projection images with different densities and rendered ground truth



### Upsample

Provide upsample benchmark data in large-scale scenes



### Segmentation

Provide unobstructed ground truth from the mesh model

Figure 2. The distinctive features of our dataset. We have innovated in five key functional areas.

several similar vehicle-mounted outdoor scene datasets [51, 53, 62] with richer classes have been released. Besides, large-scale point clouds can be obtained through airborne LiDAR scanning [54, 67, 75] or reconstruction by photogrammetry [7, 26, 35]. Semantic3D [19] employs terrestrial LiDAR to capture outdoor scenes. S3DIS [3] utilizes depth cameras to capture indoor data, resulting in denser annotated data. For synthetic datasets, SynthCity [18] is the pioneering synthetic point cloud dataset that utilizes the Blensor plugin in Blender to simulate LiDAR scanning. Paris-CARLA-3D [14] consists of real-world point clouds and synthesized point clouds, both annotated with the same categories, enabling exploration of domain transfer. SynLiDAR [66] is developed using the UE4 engine for the same motivation. STPLS3D [10] employs a 3D scene generation engine to synthesize virtual scenes, using a UAV simulator for photogrammetry and generating labeled point clouds. In comparison to these datasets, we simultaneously provide annotated point clouds obtained from scanning and the mesh model.

**Place Recognition.** There are currently a limited number of large-scale place recognition datasets available. Oxford RobotCar [40] and Mulran [29] are created using a LiDAR sensor mounted on a car that repeatedly drives through each region at different times. Our dataset simulates migration

and changes in the environment to better explore the algorithm’s robustness.

**3D Reconstruction.** LiDAR-based SLAM has become a widely adopted method for 3D reconstruction. KITTI [17] is now the most popular benchmark for odometry evaluation. The NCLT dataset [8] comprises 27 extended sequences captured by Segway platforms. The UrbanNav dataset [21] offers a challenging data source for advancing the study of accurate and robust positioning in urban canyons. Our dataset includes city-level mesh models, enabling the development of novel benchmark methods.

**3D Multi-task Dataset.** Recently, some synthetic datasets with multiple sensors have been released. KITTI-CARLA [13] utilizes sensors identical to those in the KITTI dataset within a virtual environment. AIODrive [64] is generated with a specific focus on high-density long-range LiDAR datasets. SHIFT [56] features a comprehensive sensor suite and annotations, enabling the investigation of performance degradation in perception systems as domain shift increases. These datasets are collected exclusively through CARLA. However, they meet the multi-task requirements solely by enhancing sensor configurations, lacking organization based on specific downstream tasks, or exploring relationships between different tasks.

Function	Format	Brief Description
Depth Completion	KITTI DC [58]	16/32/64/128-channal LiDAR projected image; Day&Night monocular RGB image; rendered depth ground truth.
Upsample	-	16/32/64/128-channal LiDAR scan.
Segmentation	SemanticKITTI [4]	32/64/128-channal LiDAR scan with semantic&instance label. Provide semantic-labeled point clouds obtained from the mesh model.
Place Recognition	Oxford RobotCar [40]	Monocular RGB image; rendered depth image; 64-channal LiDAR scan with pose and location. Four partially overlapping scanning routes collected before and after environmental migration.
3D Reconstruction	KITTI Odometry [17]	Stereo RGB image; rendered depth image; 64-channal LiDAR scan with pose and location. Provide city-level mesh models as ground truth.

Table 2. We organize the format of our dataset according to mainstream standards. This table contains the data items included in each task.

### 3. VEnvision3D Dataset

We have designed a data collection plan based on the requirements of mainstream point cloud tasks in the field. A comprehensive explanation of the dataset can be found in references Tab. 2 and Tab. 3.

#### 3.1. Data Collection and Annotation

To make our data more user-friendly, we have adopted some of the mainstream dataset formats. We employed a LiDAR sensor, RGB Camera, Depth Camera, and GNSS Sensor for data collection purposes. To enhance the realism of the LiDAR point clouds, two augmentation methods are employed. Firstly, points are randomly removed based on their intensity values, with a higher probability of elimination for those with lower intensities. Secondly, a selection of points is randomly perturbed along the laser ray’s direction, introducing noisy distance measurements. In response to contemporary point cloud processing research, the dataset is categorized based on various functionalities, including depth completion, segmentation, upsampling, place recognition, and 3D reconstruction. This approach facilitates ease of use and enables the exploration of connections between different tasks. Thanks to the advantages of virtual environments, data annotation can be automatically performed. We provide instance and semantic segmentation labels on 28 classes and the real depth map generated by the renderer. We also obtain semantic-labeled point clouds through Monte Carlo sampling [20] for the simulated city model, providing a new benchmark for scene-level completion, 3D reconstruction, and semantic segmentation tasks.

#### 3.2. Unique Feature

**Different density data in the same frame.** In real-world scenarios, it is challenging to obtain data with varying point densities within a single frame due to the limited availabil-

Sensor	Parameters
LiDAR	16/32/64/128-channels, 360° horizontal FoV, $-25^\circ$ to $30^\circ$ vertical FoV, 20Hz frequency, $\leq 100\text{m}$ range.
RGB Camera	Resolution of $1216 \times 352$ , FoV of $90^\circ$ , Aperture of $f/1.4$ .
Depth Camera	Same as RGB Camera.
GNSS	20Hz frequency.

Table 3. Sensor parameter settings.

ity of LiDAR sensors in vehicles. However, in our virtual environment, we have strategically placed LiDAR sensors with different channel counts (16/32/64/128 channels) at the same location. This unique configuration enables us to deliver, for the first time, scene-level point clouds with multiple densities in an upsampling task. The exploration of scene-level upsampling methods is crucial for the future development of intelligent point cloud processing. Additionally, we provide point clouds with varying densities for both depth completion and semantic segmentation tasks. These can be used to assess the algorithm’s robustness to density changes and for domain adaptation studies.

**Surface sampling from city-level model.** The existing scene-level data is obtained through LiDAR measurements, inevitably leading to the occurrence of obstructions during the collection process, making it challenging to capture the complete scene. To overcome this issue, we have employed Monte Carlo Sampling to obtain point clouds and labels from the city mesh model’s surface in our dataset. Subsequently, we have divided the entire point cloud into blocks of  $100\text{m} \times 100\text{m}$  (consistent with the LiDAR detection distance), with a cropping interval of 6m. This approach en-

asures that the blocks simulate an unobstructed effect. By adopting this method, we aim to facilitate the exploration of techniques for scene-level completion of point clouds, while previous research primarily concentrated on completing individual objects. We also believe that a city-level model can introduce innovative evaluation methods for city-scale 3D reconstruction.

**Simulate migration changes in environments.** Traditional datasets are typically obtained through a one-time acquisition process, which fails to account for temporal environmental variations such as the seasonal decay of vegetation and the evolution of construction projects. Environmental changes are crucial for the development of adaptive algorithms, yet acquiring longitudinal real-world datasets that encompass these changes is a formidable challenge, often necessitating years of data collection. To address this gap, we have employed a virtual environment to simulate the construction of buildings by selectively editing existing structures. We designed four routes, including repetitive paths and closures. Vehicles traversed these routes before and after the simulated environmental transformations, allowing us to amass datasets reflecting different environmental parameters. We envisage that such an attribute can empower researchers to more thoroughly investigate the influence of environmental changes on place recognition algorithms.

#### 4. Baseline Experiments

In this section, we tested multiple subtasks provided by VEnvision3D using the current mainstream methods. For fair comparison, we faithfully follow the experimental settings of each baseline in the original publication.

**Depth completion.** We carried out experiments on the projection maps of different channel numbers using deep learning methods [24, 45] and traditional methods [74]. Tab. 4 presents our experimental results. PENet achieved the best results, while the other two methods performed poorly. However, it should be noted that our ground truth was generated by a renderer and is denser than the annotated depth maps in the KITTI DC dataset, so the accuracy of these methods on our dataset is much lower than the results on the KITTI DC dataset. Additionally, we observed that as the LiDAR channel number increased, the accuracy of all methods improved to varying degrees, which was particularly evident in NLSPPN. This revealed the limitations of existing methods and demonstrated the enhancing effect of increasing point density on depth completion tasks. Fig. 3 shows the results of PENet for data with different point densities. It can be observed from both quantitative and visual results that with the increase in point density, there is a slight improvement in the accuracy of the completion results.

**Point cloud place recognition.** Our place recogni-

Method	Data <sup>†</sup>	RMSE	MAE	iRMSE	iMAE
NLSPPN [45]	32	6972.50	4482.53	17.61	13.47
	64	6538.66	4434.13	19.27	14.50
	128	6021.36	3714.02	16.89	12.31
	KITTI	741.68	199.59	1.99	0.84
PENet [24]	32	2833.97	803.90	7.10	2.52
	64	2808.22	782.92	6.44	2.81
	128	2724.75	739.439	9.21	2.40
	KITTI	730.08	210.55	2.17	0.94
Zhao <i>et al.</i> [74]	32	8683.49	5126.70	23.20	16.46
	64	8405.77	5001.68	23.01	16.35
	128	8283.88	4950.97	23.06	16.36
	KITTI	1239.84	298.30	3.76	1.21

Table 4. Benchmarking results of monocular depth completion on the test set. We adopt four metrics for performance evaluation, which are root mean squared error (RMSE [mm]), mean absolute error (MAE [mm]), root mean squared error of the inverse depth (iRMSE [1/km]), and mean absolute error of the inverse depth (iMAE [1/km]). <sup>†</sup>We conducted experiments using data of varying densities, including 32/64/128-channel LiDAR point cloud projection map.

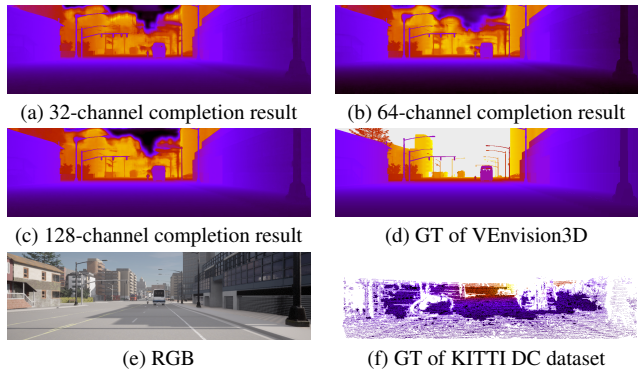


Figure 3. Depth completion results of PENet from different input(32/64/128-channel LiDAR projected image).

tion dataset used the same data preprocessing procedure as benchmark datasets proposed in [59] (except for removing ground plane points). To investigate the impact of dynamic environments, we generated four sequences before and after simulating environmental changes, denoted as Org. and Mig. respectively. Each run was split into two disjoint reference maps used for training and testing, and each reference map was organized as a set of submaps at regular intervals. We chose PointNetVLAD [59], PPTNet [28] and Min-kLoc3dv2 [32] as global feature extractors for place recognition and trained each extractor with 2 different training sets of submaps from Org. only and Org.+Mig. Regarding validation, we uniformly employed cross-validation on

all eight sequences. Tab. 5 demonstrated that training PPTNet [28] and MinkLoc3dv2 [32] with two sets of sequence data led to noticeable improvement compared to using only the original sequence. This finding highlights the influence of environmental changes on the accuracy of place recognition for the first time. The provided datasets can support ongoing research on change-robust or change-aware place recognition techniques. However, concurrent use of both training sets for PointNetVLAD resulted in a decrease in performance. We conjecture that this is due to the smaller parameter size of the network.

Method	Data <sup>†</sup>	AR@1	AR@5
PointNetVLAD [59]	Org.	87.7	90.4
	Org.+Mig.	84.3	90.3
PPTNet [28]	Org.	92.6	94.4
	Org.+Mig.	94.1	95.0
MinkLoc3dv2 [32]	Org.	89.9	94.9
	Org.+Mig.	97.1	98.5

Table 5. Benchmarking results of place recognition. Average recall at 1(AR@1 [%]) and at 5(AR@5 [%]) are reported. <sup>†</sup>Org.(Original) denotes training that exclusively utilizes data from the original environment, while Org.(Original)+Mig.(Migrated) indicates training that incorporates data from both the original and migrated environments.

**LiDAR odometry estimation.** We conducted experiments on three sequences according to the settings of KITTI Odometry. Tab. 6 presents our experimental results, where KISS-ICP [63] achieved the best results in Town05 and Town10, while A-LOAM [71] achieved the best results in Town03. However, it is unusual that MULLS [44] obtained significant deviations in Town03 and Town05, and A-LOAM’s results in Town05 were also unsatisfactory. We also tested ORB-SLAM2 [41] using stereo images, but the final performance was poor, as the algorithm lost track early in the sequence. We speculate that the reason for these low accuracy phenomena is due to the sharp turning angle in the trajectories. Overall, KISS-ICP exhibits the strongest robustness, which aligns with its characteristic of not requiring parameter tuning.

**Scene-level point cloud upsampling.** We conducted upsampling experiments using point-based [46] and transformer-based [39] methods. The results are presented in Tab. 7. It is important to mention that including the HD metric in the evaluation metrics does not effectively reveal the superiority or inferiority of the algorithm in scene-level upsampling experiments since HD only reflects the maximum mismatch between point sets. As can be seen, PU-GCN performs better in 16/32-channel input while PC2-PU is better in 64-channel input. As the density of input points increases, the accuracy of prediction results also improves.

Method	Sequence	ATE	ARE
KISS-ICP [63]	Town03	6.399	0.052
	Town05	9.583	0.069
	Town10	3.124	0.022
A-LOAM [71]	Town03	4.514	0.038
	Town05	69.811	0.402
	Town10	3.733	0.034
MULLS [44]	Town03	26.445	0.172
	Town05	228.50	1.221
	Town10	5.224	0.064

Table 6. Benchmarking results of LiDAR odometry estimation on each sequence. The errors are presented as absolute trajectory error (ATE [m]) and absolute rotational error (ARE [rad]).

This characteristic is more prominent in PC2-PU. The specific visual results are shown in Fig. 4. For the first time, we have completed the evaluation of the upsampling task on scene-level point clouds. However, from this result, it can also be seen that compared to traditional 3D object upsampling tasks, the upsampling effect at the scene level is not satisfactory. The details of some large buildings are severely lost, which poses new challenges for the point cloud upsampling task.

Method	Data <sup>†</sup>	CD	HD
PC2-PU [39]	16->128	0.255	147.641
	32->128	0.116	74.103
	64->128	0.045	48.572
PU-GCN [46]	16->128	0.124	127.608
	32->128	0.070	64.407
	64->128	0.051	46.531

Table 7. Benchmarking results of scene-level point cloud upsampling on the test set. Chamfer distance(CD) and Hausdorff distance(HD) are reported as evaluation metrics. Note that CD and HD are multiplied by  $10^3$ . <sup>†</sup>We use 16/32/64-channel LiDAR scan as input and 128-channel LiDAR scan as ground truth.

**Point cloud semantic segmentaion.** We utilized pointwise-MLP-based [25], point-convolution-based [57] and voxel-based [11] methods to test our dataset. The results are shown in Tab. 8. It can be seen that MinkowskiNet achieved the best results(voxel size is all set to 0.05). As for the pointwise-MLP-based RandLA-Net, the test results for different channel numbers are not satisfactory. For example, for small categories like traffic signs, there are even cases where the IoU is 0. We speculate that this is because the downsampling strategy used in RandLA-Net is not suitable for segmenting small objects in large scenes,

Method	Data	mIoU	car	bicycle	motorcycle	truck	other-vehicle	person	rider	road	sidewalk	ground	building	fence	vegetation	terrain	pole	traffic-sign
Minkowski U-Net [11]	32	69.0	81.8	41.7	51.1	86.1	73.1	60.6	70.3	94.0	75.8	53.4	78.9	80.0	79.5	55.6	57.8	63.9
	64	77.2	90.1	56.2	58.4	92.7	81.6	76.1	79.8	93.0	83.4	64.9	89.4	88.0	90.7	57.7	63.5	68.9
	128	82.9	95.0	73.9	76.4	95.0	76.3	84.3	82.3	93.5	86.6	63.9	95.8	93.6	95.9	60.0	80.3	73.4
RandLA-Net [25]	32	60.2	49.1	24.0	35.3	91.3	33.8	26.6	18.4	97.0	88.8	63.5	94.3	88.9	92.5	78.6	81.0	0.0
	64	69.5	66.9	26.0	53.0	96.7	82.2	56.6	1.8	98.4	92.0	73.0	97.5	94.2	96.6	87.7	89.0	0.0
	128	73.2	71.0	34.1	59.2	96.9	81.7	68.8	31.0	98.5	92.3	68.2	97.6	94.9	97.1	88.3	91.5	0.0
KPConv [57]	32	62.3	90.7	42.0	48.9	82.8	1.4	73.5	65.9	90.8	73.3	8.6	80.0	63.7	86.9	43.5	71.2	72.9
	64	76.2	95.8	64.1	65.5	91.4	27.7	84.4	76.8	92.8	80.4	49.7	91.8	87.9	94.4	53.3	80.5	82.7
	128	77.7	92.7	68.7	67.6	96.0	90.7	87.8	79.7	90.8	74.7	32.7	88.2	83.3	96.3	41.3	73.8	79.3

Table 8. Benchmarking results of point cloud semantic segmentation on the validation set. We conducted experiments on data with different point densities. Mean IoU (mIoU [%]), and per-class IoU [%] scores are reported.

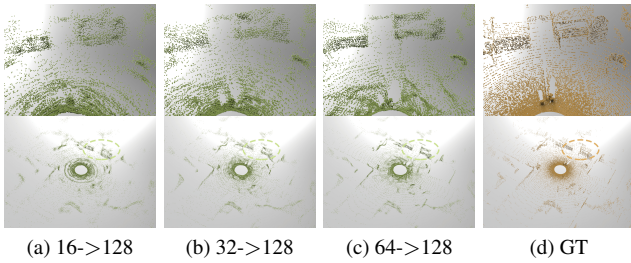


Figure 4. Upsampling results of PU-GCN from different input (16/32/64-channel LiDAR scan). The ground truth is 128-channel LiDAR scan.

resulting in performance degradation. In point-convolution-based KPConv, compared to the 64-channel data, the 128-channel data did not show a significant improvement. This is because, for the KPConv, with higher-density input point clouds, precise adjustment of the neighborhood radius is essential to prevent performance degradation. The multi-density point clouds we offer facilitate robustness testing of semantic segmentation algorithms across domains, aiding researchers in exploring domain adaptation or generalization studies.

## 5. Multi-task Exploration

In this section, we take upsampling and segmentation as examples to investigate the mutual reinforcement between different tasks, demonstrating the crucial role of multi-task learning in 3D scene understanding. Based on the results, we discuss the potential of our dataset in establishing end-to-end foundation models within the 3D vision field.

### 5.1. The Network

We adopt PU-Dense [2] network architecture as the backbone network and extend a branch for semantic segmenta-

tion task. The detailed network architecture is illustrated in Fig. 5. Apart from the original PU-Dense structure, we incorporate transposed convolution [11] to upsample features from different scales of the encoder. These features are then concatenated as input, and the SENet [22] is applied to learn the importance of each channel. Ultimately, a linear classifier is employed to accomplish the semantic segmentation. Besides, we adjusted the expansion factor (kernel size) for coordinate generation within the PU-Dense network to accommodate large-scale scenes.

### 5.2. Loss Function

For the upsampling branch, we employ a voxel-based BCE Loss consistent with PU-Dense, while for the semantic segmentation branch, we use the conventional CE Loss. The final loss for the entire network is the average of these values, with the detailed definition as follows:

$$\mathcal{L}_{BCE} = -\frac{1}{N} \sum_i (x_i \log(p_i) + (1 - x_i) \log(1 - p_i)) \quad (1)$$

$$\mathcal{L}_{CE} = -\frac{1}{N} \sum_i x_i \log(p_i) \quad (2)$$

$$\mathcal{L} = \frac{1}{2} \mathcal{L}_{BCE} + \frac{1}{2} \mathcal{L}_{CE} \quad (3)$$

In  $\mathcal{L}_{BCE}$ ,  $x_i$  is the voxel label that is either occupied (1) or empty (0) in the GT point cloud.  $p_i$  is the probability of the voxel being occupied and is calculated using a *sigmoid* function applied to the decoder output  $D_0$ . In  $\mathcal{L}_{CE}$ ,  $x_i$  refers to the one-hot label entry, and  $p_i$  represents the probability of a point being predicted as a certain class.

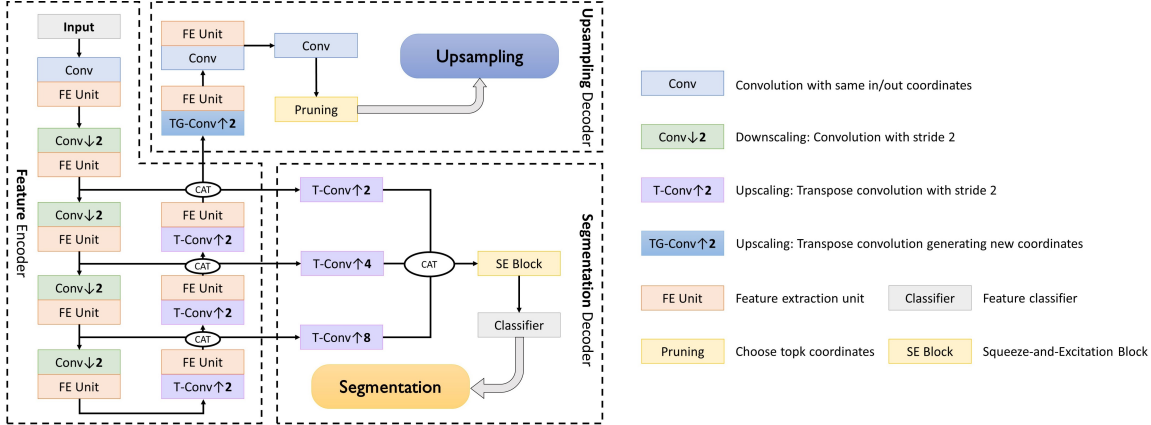


Figure 5. Multi-task end-to-end network architecture. We adopt PU-Dense as the backbone network architecture and expand it with a semantic segmentation branch.

### 5.3. Experiments

To explore the relationships between multiple subtasks, we adopt the following experimental strategies: training solely with the upsampling branch; training solely with the semantic segmentation branch; and simultaneous training with both the upsampling and semantic segmentation branches. Such a design allows us to quantify the phenomena of inter-task influence, providing a research basis for the design of end-to-end foundation models.

Using data with different point densities from our dataset, we take the coordinate values of the 32-channel point cloud as input, the 128-channel point cloud as the ground truth for upsampling, and the label values of the 32-channel point cloud as the ground truth for semantic segmentation. For a fair comparison, the Adam [30] and SGD [52] optimizer is used with a weight decay of 0.0001 and a default learning rate of 0.002. We use exponentialLR [36] to adjust learning rate and the gamma is 0.5. During the training procedure, random rotation along z-axis is performed for the augmentation. The model is trained for 5 epochs with a batch size of 4 under each setting.

Branch	Ups. AR	Ups. CD	Seg. mIoU
Ups.	43.2	45.5	-
Seg.	-	-	43.6
Ups+Seg.	46.5	43.1	45.3

Table 9. We conducted experiments on the upsampling branch(Ups.), the semantic segmentation branch(Seg.), and both branches simultaneously(Ups.+Seg.). Chamfer distance(CD, multiplied by  $10^3$ ) and average recall(AR [%]) is reported as evaluation metrics for upsamplng and mean IOU(mIoU [%]) is reported for semantic segmentation.

The experimental results are shown in Tab. 9. From the experimental results, it can be observed that when the upsampling and segmentation branches are conducted simultaneously, both the Average Recall (AR) of the upsampling task and the mean Intersection over Union (mIoU) of the segmentation task show improvement. They increased from 43.2% to 46.5% and from 43.6% to 45.3%, respectively. Such results demonstrate the phenomenon of mutual promotion among specific downstream subtasks. The upsampling task forces the encoder to capture the implicit surface structure of objects, and such information can provide geometric constraints for semantic segmentation. Conversely, the semantic information provided by the semantic segmentation task can also assist the upsampling task in obtaining category-related information, thereby improving the upsampling process. It is worth noting that the Chamfer Distance (CD) does not meet the expected performance as PU-Dense is a voxel-based method that achieves upsampling by expanding the voxels occupied by the original spatial points. So it does not adequately reflect the quality of the upsampling.

Through simple experimental setups, we can leverage the proposed dataset for multi-task learning. This demonstrates the advantage of collecting the dataset from the same scenarios, allowing for the convenient integration of multiple tasks without the need for complex mappings. This also reflects that our dataset can support the exploration of an end-to-end multi-task framework.

## 6. Conclusion

We introduce VEnvision3D, a synthetic perception dataset featuring the exploration of 3D multi-task models, including depth completion, segmentation, upsample, place recognition, and 3D reconstruction. In a virtual environment, we have implemented innovative sensor configurations, endowing our dataset with unique charac-

teristics. For instance, it can provide data with varying densities within the same frame, offer surface-sampled data at a city level, and simulate environmental changes. These features aim to contribute to the advancement of the field of point cloud perception. In addition, benefiting from the carefully designed settings in our data collection, we have integrated the upsampling task and semantic segmentation task into a multi-task framework. Through experiments, we have demonstrated the mutually beneficial relationship among different subtasks. In summary, by introducing this dataset, we hope to provide researchers with a platform to study unified multi-task models, thereby advancing the development of foundation models in the 3D vision field.

## References

- [1] Papers with code. <https://paperswithcode.com/>. **2**
- [2] Anique Akhtar, Zhu Li, Geert Van der Auwera, Li Li, and Jianle Chen. Pu-dense: Sparse tensor-based point cloud geometry upsampling. *IEEE Transactions on Image Processing*, 31:4133–4148, 2022. **7**
- [3] I. Armeni, A. Sax, A. R. Zamir, and S. Savarese. Joint 2D-3D-Semantic Data for Indoor Scene Understanding. *ArXiv e-prints*, 2017. **2, 3**
- [4] J. Behley, M. Garbade, A. Milioto, J. Quenzel, S. Behnke, C. Stachniss, and J. Gall. SemanticKITTI: A Dataset for Semantic Scene Understanding of LiDAR Sequences. In *Proc. of the IEEE/CVF International Conf. on Computer Vision (ICCV)*, 2019. **1, 2, 4**
- [5] Federica Bogo, Javier Romero, Matthew Loper, and Michael J Black. Faust: Dataset and evaluation for 3d mesh registration. In *Proceedings of the IEEE conference on computer vision and pattern recognition*, pages 3794–3801, 2014. **2**
- [6] Rishi Bommasani, Drew A Hudson, Ehsan Adeli, Russ Altman, Simran Arora, Sydney von Arx, Michael S Bernstein, Jeannette Bohg, Antoine Bosselut, Emma Brunskill, et al. On the opportunities and risks of foundation models. *arXiv preprint arXiv:2108.07258*, 2021. **1**
- [7] Gülcan Can, Dario Mantegazza, Gabriele Abbate, Sébastien Chappuis, and Alessandro Giusti. Semantic segmentation on swiss3dcities: A benchmark study on aerial photogrammetric 3d pointcloud dataset. *Pattern Recognition Letters*, 150: 108–114, 2021. **3**
- [8] Nicholas Carlevaris-Bianco, Arash K. Ushani, and Ryan M. Eustice. University of Michigan North Campus long-term vision and lidar dataset. *International Journal of Robotics Research*, 35(9):1023–1035, 2015. **3**
- [9] Angel X. Chang, Thomas Funkhouser, Leonidas Guibas, Pat Hanrahan, Qixing Huang, Zimo Li, Silvio Savarese, Manolis Savva, Shuran Song, Hao Su, Jianxiong Xiao, Li Yi, and Fisher Yu. ShapeNet: An Information-Rich 3D Model Repository. Technical Report arXiv:1512.03012 [cs.GR], Stanford University — Princeton University — Toyota Technological Institute at Chicago, 2015. **1, 2**
- [10] Meida Chen, Qingyong Hu, Zifan Yu, Hugues THOMAS, Andrew Feng, Yu Hou, Kyle McCullough, Fengbo Ren, and Lucio Soibelman. Stpls3d: A large-scale synthetic and real aerial photogrammetry 3d point cloud dataset. In *33rd British Machine Vision Conference 2022, BMVC 2022, London, UK, November 21-24, 2022*. BMVA Press, 2022. **2, 3**
- [11] Christopher Choy, JunYoung Gwak, and Silvio Savarese. 4d spatio-temporal convnets: Minkowski convolutional neural networks. In *Proceedings of the IEEE Conference on Computer Vision and Pattern Recognition*, pages 3075–3084, 2019. **6, 7**
- [12] Jia Deng, Wei Dong, Richard Socher, Li-Jia Li, Kai Li, and Li Fei-Fei. Imagenet: A large-scale hierarchical image database. In *2009 IEEE conference on computer vision and pattern recognition*, pages 248–255. Ieee, 2009. **1**
- [13] Jean-Emmanuel Deschaud. KITTI-CARLA: a KITTI-like dataset generated by CARLA Simulator. *arXiv e-prints*, art. arXiv:2109.00892, 2021. **2, 3**
- [14] Jean-Emmanuel Deschaud, David Duque, Jean Pierre Richa, Santiago Velasco-Forero, Beatriz Marcotegui, and François Goulette. Paris-carla-3d: A real and synthetic outdoor point cloud dataset for challenging tasks in 3d mapping. *Remote Sensing*, 13(22), 2021. **3**
- [15] Alexey Dosovitskiy, German Ros, Felipe Codevilla, Antonio Lopez, and Vladlen Koltun. CARLA: An open urban driving simulator. In *Proceedings of the 1st Annual Conference on Robot Learning*, pages 1–16, 2017. **2**
- [16] Chris Fifty, Ehsan Amid, Zhe Zhao, Tianhe Yu, Rohan Anil, and Chelsea Finn. Efficiently identifying task groupings for multi-task learning. *Advances in Neural Information Processing Systems*, 34:27503–27516, 2021. **1**
- [17] Andreas Geiger, Philip Lenz, Christoph Stiller, and Raquel Urtasun. Vision meets robotics: The kitti dataset. *International Journal of Robotics Research (IJRR)*, 2013. **1, 2, 3, 4**
- [18] David Griffiths and Jan Boehm. SynthCity: A large scale synthetic point cloud. In *ArXiv preprint*, 2019. **2, 3**
- [19] Timo Hackel, N. Savinov, L. Ladicky, Jan D. Wegner, K. Schindler, and M. Pollefeys. SEMANTIC3D.NET: A new large-scale point cloud classification benchmark. In *ISPRS Annals of the Photogrammetry, Remote Sensing and Spatial Information Sciences*, pages 91–98, 2017. **3**
- [20] W Keith Hastings. Monte carlo sampling methods using markov chains and their applications. 1970. **4**
- [21] Li-Ta Hsu, Nobuaki Kubo, Weisong Wen, Wu Chen, Zhizhao Liu, Taro Suzuki, and Junichi Meguro. Urbannav: An open-sourced multisensory dataset for benchmarking positioning algorithms designed for urban areas. In *Proceedings of the 34th International Technical Meeting of the Satellite Division of The Institute of Navigation (ION GNSS+ 2021)*, pages 226–256, 2021. **3**
- [22] Jie Hu, Li Shen, and Gang Sun. Squeeze-and-excitation networks. 2018. **7**
- [23] Junjie Hu, Chenyu Bao, Mete Ozay, Chenyou Fan, Qing Gao, Honghai Liu, and Tin Lun Lam. Deep depth completion from extremely sparse data: A survey. *IEEE Transactions on Pattern Analysis and Machine Intelligence*, 2022. **2**
- [24] Mu Hu, Shuling Wang, Bin Li, Shiyu Ning, Li Fan, and Xiaojin Gong. Towards precise and efficient image guided depth completion. 2021. **5**

- [25] Qingyong Hu, Bo Yang, Linhai Xie, Stefano Rosa, Yulan Guo, Zihua Wang, Niki Trigoni, and Andrew Markham. Randla-net: Efficient semantic segmentation of large-scale point clouds. *Proceedings of the IEEE Conference on Computer Vision and Pattern Recognition*, 2020. 6, 7
- [26] Qingyong Hu, Bo Yang, Sheikh Khalid, Wen Xiao, Niki Trigoni, and Andrew Markham. Towards semantic segmentation of urban-scale 3d point clouds: A dataset, benchmarks and challenges. In *Proceedings of the IEEE/CVF Conference on Computer Vision and Pattern Recognition*, 2021. 3
- [27] Yihan Hu, Jiazhi Yang, Li Chen, Keyu Li, Chonghao Sima, Xizhou Zhu, Siqi Chai, Senyao Du, Tianwei Lin, Wenhai Wang, et al. Planning-oriented autonomous driving. In *Proceedings of the IEEE/CVF Conference on Computer Vision and Pattern Recognition*, pages 17853–17862, 2023. 1
- [28] Le Hui, Hang Yang, Mingmei Cheng, Jin Xie, and Jian Yang. Pyramid point cloud transformer for large-scale place recognition. In *ICCV*, 2021. 5, 6
- [29] Giseop Kim, Yeong Sang Park, Younghun Cho, Jinyong Jeong, and Ayoung Kim. Mulran: Multimodal range dataset for urban place recognition. In *Proceedings of the IEEE International Conference on Robotics and Automation (ICRA)*, Paris, 2020. 3
- [30] Diederik P Kingma and Jimmy Ba. Adam: A method for stochastic optimization. *arXiv preprint arXiv:1412.6980*, 2014. 8
- [31] Alexander Kirillov, Eric Mintun, Nikhila Ravi, Hanzi Mao, Chloe Rolland, Laura Gustafson, Tete Xiao, Spencer Whitehead, Alexander C. Berg, Wan-Yen Lo, Piotr Dollár, and Ross Girshick. Segment anything. *arXiv:2304.02643*, 2023. 1
- [32] Jacek Komorowski. Improving point cloud based place recognition with ranking-based loss and large batch training. In *2022 26th International Conference on Pattern Recognition (ICPR)*, pages 3699–3705, 2022. 5, 6
- [33] Matthew Le, Apoorv Vyas, Bowen Shi, Brian Karrer, Leda Sari, Rashel Moritz, Mary Williamson, Vimal Manohar, Yossi Adi, Jay Mahadeokar, et al. Voicebox: Text-guided multilingual universal speech generation at scale. *arXiv preprint arXiv:2306.15687*, 2023. 1
- [34] Ruihui Li, Xianzhi Li, Chi-Wing Fu, Daniel Cohen-Or, and Pheng-Ann Heng. Pu-gan: a point cloud upsampling adversarial network. In *Proceedings of the IEEE/CVF international conference on computer vision*, pages 7203–7212, 2019. 2
- [35] Xinke Li, Chongshou Li, Zekun Tong, Andrew Lim, Junsong Yuan, Yuwei Wu, Jing Tang, and Raymond Huang. Campus3d: A photogrammetry point cloud benchmark for hierarchical understanding of outdoor scene. In *Proceedings of the 28th ACM International Conference on Multimedia*, pages 238–246, 2020. 3
- [36] Zhiyuan Li and Sanjeev Arora. An exponential learning rate schedule for deep learning. *arXiv preprint arXiv:1910.07454*, 2019. 8
- [37] Tsung-Yi Lin, Michael Maire, Serge Belongie, James Hays, Pietro Perona, Deva Ramanan, Piotr Dollár, and C Lawrence Zitnick. Microsoft coco: Common objects in context. In *Computer Vision—ECCV 2014: 13th European Conference, Zurich, Switzerland, September 6–12, 2014, Proceedings, Part V 13*, pages 740–755. Springer, 2014. 1
- [38] Ziwei Liu, Ping Luo, Xiaogang Wang, and Xiaoou Tang. Deep learning face attributes in the wild. In *Proceedings of International Conference on Computer Vision (ICCV)*, 2015. 1
- [39] Chen Long, WenXiao Zhang, Ruihui Li, Hao Wang, Zhen Dong, and Bisheng Yang. Pc2-pu: Patch correlation and point correlation for effective point cloud upsampling. In *Proceedings of the 30th ACM International Conference on Multimedia*, pages 2191–2201, 2022. 6
- [40] Will Maddern, Geoff Pascoe, Chris Linegar, and Paul Newman. 1 Year, 1000km: The Oxford RobotCar Dataset. *The International Journal of Robotics Research (IJRR)*, 36(1):3–15, 2017. 2, 3, 4
- [41] Raúl Mur-Artal and Juan D. Tardós. ORB-SLAM2: an open-source SLAM system for monocular, stereo and RGB-D cameras. *IEEE Transactions on Robotics*, 33(5):1255–1262, 2017. 6
- [42] OpenAI. Gpt-4 technical report, 2023. 1
- [43] Long Ouyang, Jeffrey Wu, Xu Jiang, Diogo Almeida, Carroll Wainwright, Pamela Mishkin, Chong Zhang, Sandhini Agarwal, Katarina Slama, Alex Ray, et al. Training language models to follow instructions with human feedback. *Advances in Neural Information Processing Systems*, 35: 27730–27744, 2022. 1
- [44] Yue Pan, Pengchuan Xiao, Yujie He, Zhenlei Shao, and Zesong Li. Mulls: Versatile lidar slam via multi-metric linear least square. In *2021 IEEE International Conference on Robotics and Automation (ICRA)*, pages 11633–11640. IEEE, 2021. 6
- [45] Jinsun Park, Kyungdon Joo, Zhe Hu, Chi-Kuei Liu, and In So Kweon. Non-local spatial propagation network for depth completion. In *Proc. of European Conference on Computer Vision (ECCV)*, 2020. 5
- [46] Guocheng Qian, Abdullellah Abualshour, Guohao Li, Ali Thabet, and Bernard Ghanem. Pu-gcn: Point cloud upsampling using graph convolutional networks. In *Proceedings of the IEEE/CVF Conference on Computer Vision and Pattern Recognition (CVPR)*, pages 11683–11692, 2021. 2, 6
- [47] Yue Qian, Junhui Hou, Sam Kwong, and Ying He. Pugeonet: A geometry-centric network for 3d point cloud upsampling. In *European conference on computer vision*, pages 752–769. Springer, 2020. 2
- [48] Jiaxiong Qiu, Zhaopeng Cui, Yinda Zhang, Xingdi Zhang, Shuaicheng Liu, Bing Zeng, and Marc Pollefeys. Deeplidar: Deep surface normal guided depth prediction for outdoor scene from sparse lidar data and single color image. In *The IEEE Conference on Computer Vision and Pattern Recognition (CVPR)*, 2019. 2
- [49] Alec Radford, Jong Wook Kim, Chris Hallacy, Aditya Ramesh, Gabriel Goh, Sandhini Agarwal, Girish Sastry, Amanda Askell, Pamela Mishkin, Jack Clark, et al. Learning transferable visual models from natural language supervision. In *International conference on machine learning*, pages 8748–8763. PMLR, 2021. 1

- [50] Aditya Ramesh, Prafulla Dhariwal, Alex Nichol, Casey Chu, and Mark Chen. Hierarchical text-conditional image generation with clip latents. *arXiv preprint arXiv:2204.06125*, 2022. 1
- [51] Xavier Roynard, Jean-Emmanuel Deschaud, and François Goulette. Paris-lille-3d: A large and high-quality ground-truth urban point cloud dataset for automatic segmentation and classification. *The International Journal of Robotics Research*, 37(6):545–557, 2018. 3
- [52] Sebastian Ruder. An overview of gradient descent optimization algorithms. *arXiv preprint arXiv:1609.04747*, 2016. 8
- [53] Andrés Serna, Beatriz Marcotegui, François Goulette, and Jean-Emmanuel Deschaud. Paris-rue-madame database: a 3d mobile laser scanner dataset for benchmarking urban detection, segmentation and classification methods. In *4th international conference on pattern recognition, applications and methods ICPRAM 2014*, 2014. 3
- [54] Nina M. Singer and Vijayan K. Asari. Dales objects: A large scale benchmark dataset for instance segmentation in aerial lidar. *IEEE Access*, pages 1–1, 2021. 3
- [55] Trevor Standley, Amir Zamir, Dawn Chen, Leonidas Guibas, Jitendra Malik, and Silvio Savarese. Which tasks should be learned together in multi-task learning? In *International Conference on Machine Learning*, pages 9120–9132. PMLR, 2020. 1
- [56] Tao Sun, Mattia Segu, Janis Postels, Yuxuan Wang, Luc Van Gool, Bernt Schiele, Federico Tombari, and Fisher Yu. SHIFT: a synthetic driving dataset for continuous multi-task domain adaptation. In *Proceedings of the IEEE/CVF Conference on Computer Vision and Pattern Recognition (CVPR)*, pages 21371–21382, 2022. 2, 3
- [57] Hugues Thomas, Charles R. Qi, Jean-Emmanuel Deschaud, Beatriz Marcotegui, François Goulette, and Leonidas J. Guibas. Kpconv: Flexible and deformable convolution for point clouds. *Proceedings of the IEEE International Conference on Computer Vision*, 2019. 6, 7
- [58] Jonas Uhrig, Nick Schneider, Lukas Schneider, Uwe Franke, Thomas Brox, and Andreas Geiger. Sparsity invariant cnns. In *International Conference on 3D Vision (3DV)*, 2017. 2, 4
- [59] Mikaela Angelina Uy and Gim Hee Lee. Pointnetvlad: Deep point cloud based retrieval for large-scale place recognition. In *The IEEE Conference on Computer Vision and Pattern Recognition (CVPR)*, 2018. 5, 6
- [60] Mikaela Angelina Uy, Quang-Hieu Pham, Binh-Son Hua, Duc Thanh Nguyen, and Sai-Kit Yeung. Revisiting point cloud classification: A new benchmark dataset and classification model on real-world data. In *International Conference on Computer Vision (ICCV)*, 2019. 2
- [61] Partoo Vafaeikia, Khashayar Namdar, and Farzad Khalvati. A brief review of deep multi-task learning and auxiliary task learning. *arXiv preprint arXiv:2007.01126*, 2020. 1
- [62] Bruno Vallet, Mathieu Brédif, Andrés Serna, Beatriz Marcotegui, and Nicolas Paparoditis. Terramobilita/iqmulus urban point cloud analysis benchmark. *Computers & Graphics*, 49:126–133, 2015. 3
- [63] Ignacio Vizzo, Tiziano Guadagnino, Benedikt Mersch, Louis Wiesmann, Jens Behley, and Cyrill Stachniss. KISS-ICP: In Defense of Point-to-Point ICP – Simple, Accurate, and Robust Registration If Done the Right Way. *IEEE Robotics and Automation Letters (RA-L)*, 8(2):1029–1036, 2023. 6
- [64] Xinshuo Weng, Yunze Man, Jinhyung Park, Ye Yuan, Dazhi Cheng, Matthew O’Toole, and Kris Kitani. All-In-One Drive: A Large-Scale Comprehensive Perception Dataset with High-Density Long-Range Point Clouds. *arXiv*, 2021. 2, 3
- [65] Zhirong Wu, Shuran Song, Aditya Khosla, Fisher Yu, Linguang Zhang, Xiaoou Tang, and Jianxiong Xiao. 3d shapenets: A deep representation for volumetric shapes. In *Proceedings of the IEEE conference on computer vision and pattern recognition*, pages 1912–1920, 2015. 2
- [66] Aoran Xiao, Jiaying Huang, Dayan Guan, Fangneng Zhan, and Shijian Lu. Transfer learning from synthetic to real lidar point cloud for semantic segmentation. In *Proceedings of the AAAI Conference on Artificial Intelligence*, pages 2795–2803, 2022. 3
- [67] Zhen Ye, Yusheng Xu, Rong Huang, Xiaohua Tong, Xin Li, Xiangfeng Liu, Kuifeng Luan, Ludwig Hoegner, and Uwe Stilla. Lasdu: A large-scale aerial lidar dataset for semantic labeling in dense urban areas. *ISPRS International Journal of Geo-Information*, 9(7):450, 2020. 3
- [68] Lequan Yu, Xianzhi Li, Chi-Wing Fu, Daniel Cohen-Or, and Pheng-Ann Heng. Ec-net: an edge-aware point set consolidation network. In *Proceedings of the European conference on computer vision (ECCV)*, pages 386–402, 2018. 2
- [69] Lequan Yu, Xianzhi Li, Chi-Wing Fu, Daniel Cohen-Or, and Pheng-Ann Heng. Pu-net: Point cloud upsampling network. In *Proceedings of the IEEE conference on computer vision and pattern recognition*, pages 2790–2799, 2018. 2
- [70] Qingyang Yu, Lei Chu, Qi Wu, and Ling Pei. Grayscale and normal guided depth completion with a low-cost lidar. In *2021 IEEE International Conference on Image Processing (ICIP)*, pages 979–983. IEEE, 2021. 2
- [71] Ji Zhang and Sanjiv Singh. Loam: Lidar odometry and mapping in real-time. In *Robotics: Science and systems*, pages 1–9. Berkeley, CA, 2014. 6
- [72] Yu Zhang and Qiang Yang. An overview of multi-task learning. *National Science Review*, 5(1):30–43, 2018. 1
- [73] Wayne Xin Zhao, Kun Zhou, Junyi Li, Tianyi Tang, XiaoLei Wang, Yupeng Hou, Yingqian Min, Beichen Zhang, Junjie Zhang, Zican Dong, et al. A survey of large language models. *arXiv preprint arXiv:2303.18223*, 2023. 1
- [74] Yiming Zhao, Lin Bai, Ziming Zhang, and Xinming Huang. A surface geometry model for lidar depth completion. *IEEE Robotics and Automation Letters*, 6(3):4457–4464, 2021. 5
- [75] SM Zolanvari, Susana Ruano, Aakanksha Rana, Alan Cummins, Rogerio Eduardo da Silva, Morteza Rahbar, and Aljosa Smolic. Dublincity: Annotated lidar point cloud and its applications. *arXiv preprint arXiv:1909.03613*, 2019. 3

# VENvision3D: A Synthetic Perception Dataset for 3D Multi-Task Model Research

## Supplementary Material

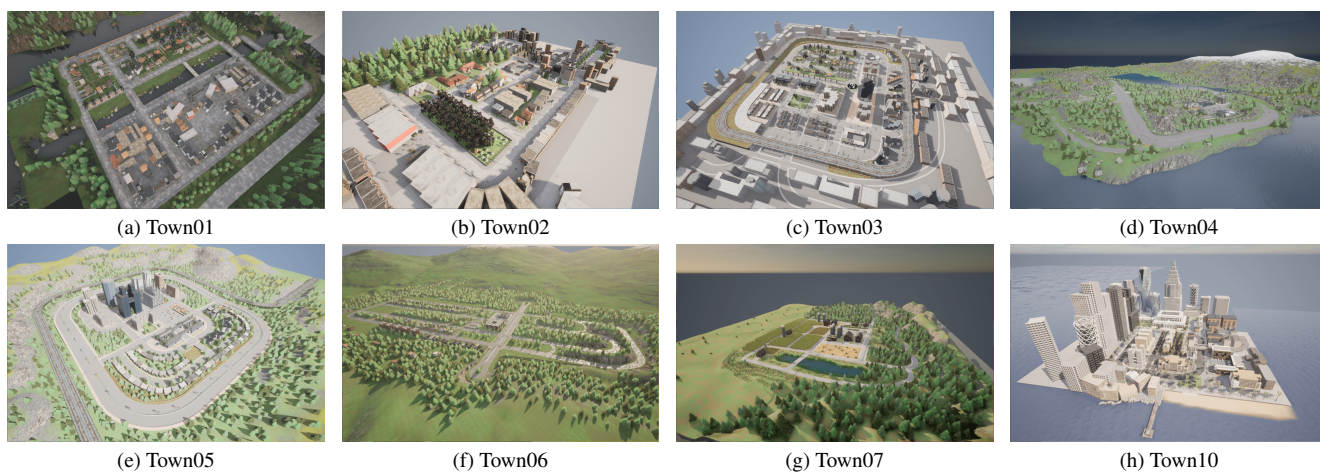


Figure 6. The 8 city maps used during the collection process.

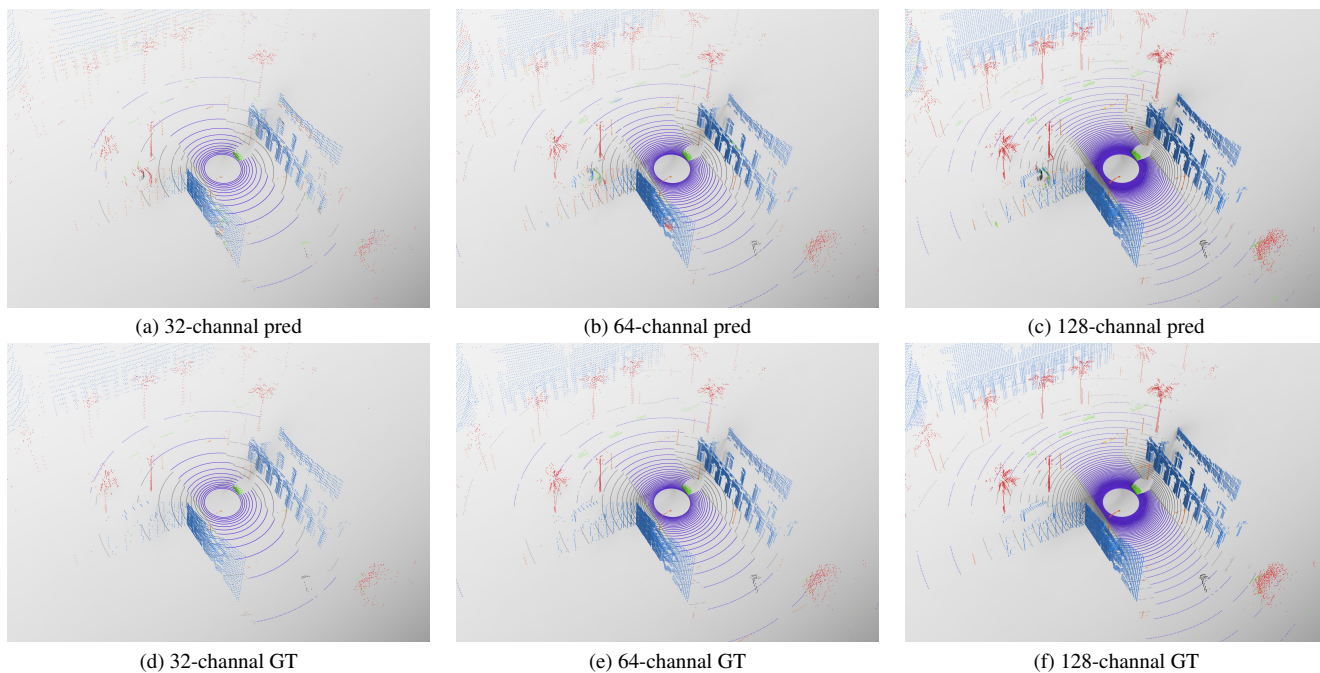


Figure 7. Semantic segmentation results of Minkowski U-Net from different input(32/64/128-channal LiDAR scan).

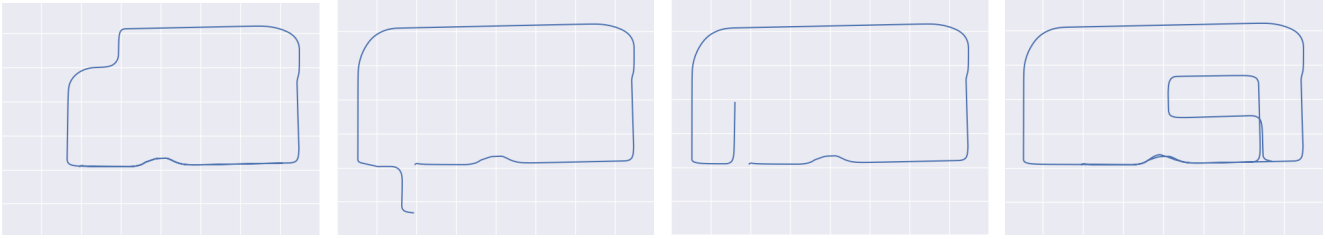


Figure 8. Visualization results of the designed 4 routes in point cloud place recognition task.

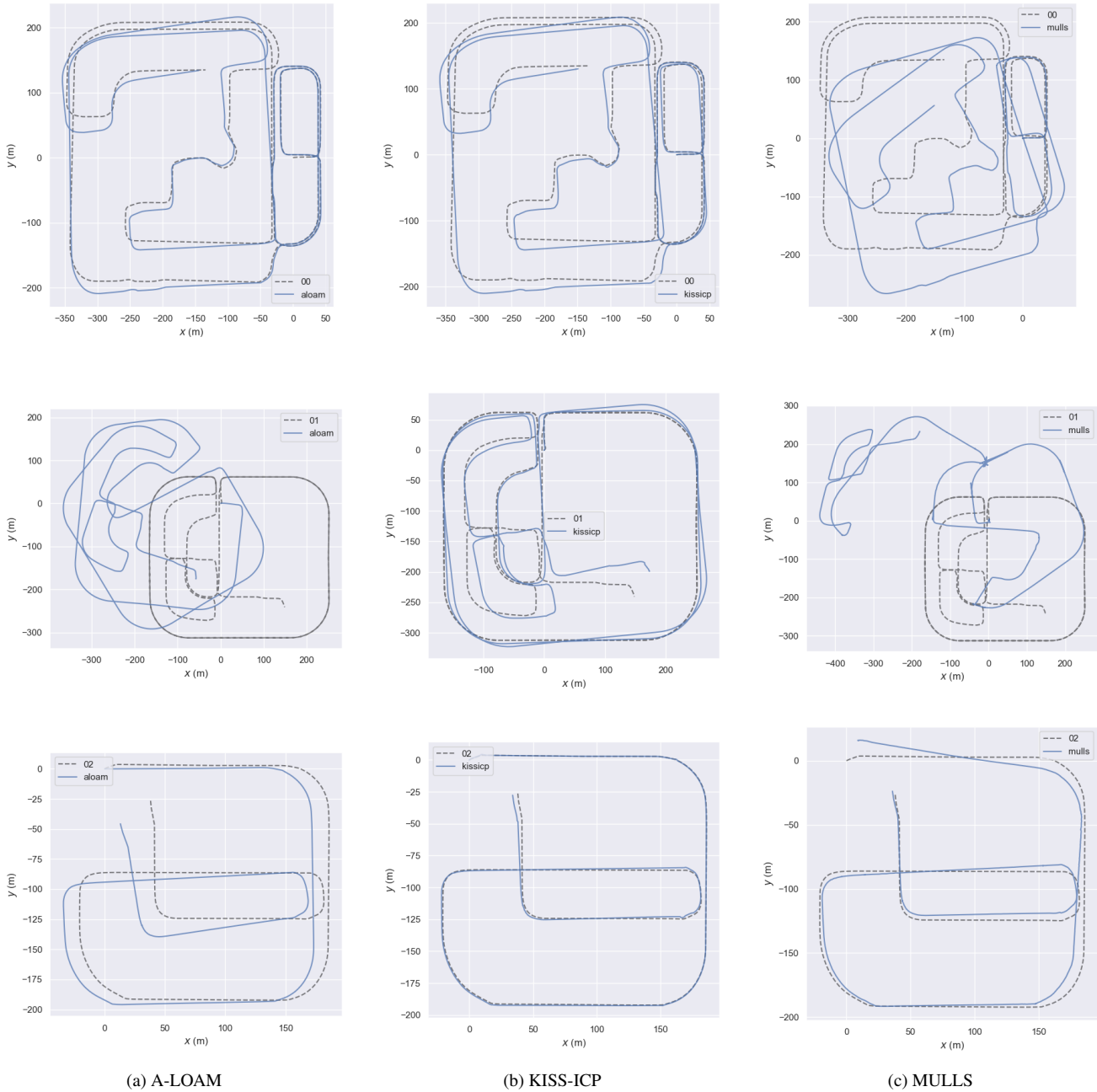


Figure 9. Visualization results of LiDAR odometry estimation on each sequence. Note that 00 refers to sequence Town03, 01 refers to sequence Town05 and 02 refers to sequence Town10.